



Disulfiram-loaded functionalized magnetic nanoparticles combined with copper and sodium nitroprusside in breast cancer cells

Kübra Solak^{a,*}, Ahmet Mavi^{a,b}, Bilal Yılmaz^c

^a Department of Nanoscience and Nanoengineering, Institute of Science, Atatürk University, 25240 Erzurum, Turkey

^b Department of Mathematics and Science Education, Education Faculty of Kazım Karabekir, Atatürk University, 25240 Erzurum, Turkey

^c Department of Analytical Chemistry, Faculty of Pharmacy, Atatürk University, 25240 Erzurum, Turkey



ARTICLE INFO

Keywords:

Fe₃O₄
Mesoporous silica nanoparticles
Disulfiram
Diethyldithiocarbamate
Sodium nitroprusside
Copper
Cancer

ABSTRACT

Disulfiram (DSF), one of the members of the dithiocarbamate family, is a reactive species (RS) generator and is capable of inducing cancer cell death in breast cancer. However, it is hydrophobic and highly degradable in blood. Therefore, drug delivery systems would be of great benefit in supporting the selective accumulation of DSF in tumor cells. In this study, it was aimed to prepare a drug carrier system based on magnetic mesoporous silica nanoparticles (Fe₃O₄@mSiO₂ MNPs) which are non-toxic, biocompatible, and have a mesoporous structure. The Fe₃O₄@mSiO₂ MNPs were modified with folic acid linked polyethyleneimine (PEI-FA) to increase both their solubility in water and specificity for cancer cells. Thus, the cancer-selective DSF-carrier system (mMDPF) was synthesized with a high surface area but with dimensions of less than 160 nm, and were characterized by dynamic light scattering (DLS), transmission electron microscopy (TEM) and Brunauer-Emmett-Teller (BET) analysis. The drug-loading capacity of mMDPF was measured as 4.35% by high-performance liquid chromatography (HPLC) and the best drug release kinetics of mMDPF was observed at 37 °C and pH 6.0 which is the pH in the endosome. The cytotoxicity of the mMDPF on breast cancer (MCF-7) cells was improved by applying mMDPF with copper and/or sodium nitroprusside. It was observed that mMDPF was taken up more by MCF-7 cells and its toxicity on MCF-7 cells was much higher than non-tumorigenic (MCF-10A) cells.

1. Introduction

Many types of cancer cell are characterized by a high level of reactive species (RS) and increased expression of antioxidant enzymes to promote cell proliferation, differentiation and oncogene activity [1]. On the other hand, increased RS concentration provokes oxidative damage to cells by altering double bonds of lipids, proteins, and DNA. The intracellular levels of RS are kept in balance to encourage cells from oxidative stress via the antioxidant system under normal physiological conditions [1]. Superoxide dismutase (SOD, EC 1.15.1.1) is one of the scavengers that regulates RS levels by catalyzing the conversion of the superoxide radical (O₂⁻) into molecular oxygen (O₂) and hydrogen peroxide (H₂O₂). H₂O₂ is removed by catalase and peroxidase enzymes (Scheme 1). Hereby, specific inhibitors of antioxidant enzymes and RS-generating agents have been suggested as cancer therapeutic agents.

Disulfiram (DSF) is a SOD inhibitor and has been used for years for treating alcoholism under the trade name Antabuse [2]. It works in that role via an irreversible inhibition of aldehyde dehydrogenase (ALDH). DSF induces oxidative stress, apoptosis, cell cycle arrest and p-glycoprotein inhibition and also reduces cancer cell proliferation, angiogenesis, tumor metastasis, multi-drug resistance, and proteasome and NF-κB activity [3–7]. Interestingly, DSF shows anti-cancer potency but its anti-cancer mechanism is not fully understood. However, using DSF against cancer is limited because of its rapid degradation in the body and its low solubility in water. Consequently, a variety of delivery systems have been used as DSF carriers such as polymeric micelles, poly lactic-co-glycolic acid and lipid emulsions [8–10].

Mesoporous silica nanoparticles (MSPs) are nanotechnology-based drug delivery systems that are used in several application areas such as labeling, separation of molecules, and tissue-specific release of

Abbreviations: ALDH, Aldehyde dehydrogenase; BET, Brunauer-Emmett-Teller; BJH, Barrett-Joyner-Halenda; Cu²⁺, Copper; DLS, Dynamic light scattering; DSF, Disulfiram; Fe₃O₄@mSiO₂ MNPs, Magnetic mesoporous silica nanoparticles; FTIR, Fourier-transform infrared spectroscopy; HPLC, High-performance liquid chromatography; mMDPF, DSF-loaded mMPF; mMPF, PEI-FA-functionalized Fe₃O₄@mSiO₂ MNPs; MSPs, Mesoporous silica nanoparticles; PEI-FA, Folic acid linked polyethyleneimine; RS, Reactive Species; SEM, Scanning electron microscopy; SNP, Sodium nitroprusside; TEM, Transmission electron microscopy; XRD, X-ray diffraction

* Corresponding author.

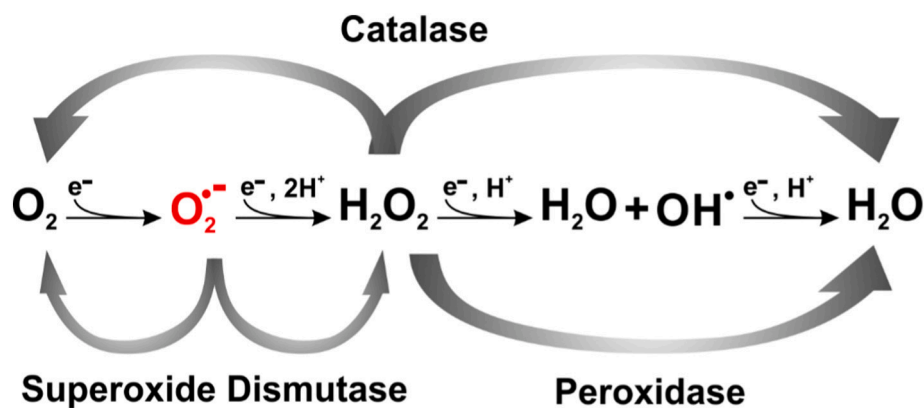
E-mail address: kubra.solak@ogr.atauni.edu.tr (K. Solak).

<https://doi.org/10.1016/j.msec.2020.111452>

Received 5 May 2020; Received in revised form 18 August 2020; Accepted 25 August 2020

Available online 27 August 2020

0928-4931/ © 2020 Elsevier B.V. All rights reserved.



Scheme 1. Activity of catalase, superoxide dismutase, and peroxidase.

therapeutic agents such as drugs, DNA, RNA, oligonucleotides, proteins or enzymes [11,12]. MSPs have been used to loading of small molecules [13]. Biocompatible MSPs exhibit excellent colloidal stability, minimize undesired protein adsorption on the surface and have high drug loading capacity with high surface areas ($> 700 \text{ m}^2/\text{g}$) and pore volumes ($> 1 \text{ cm}^3/\text{g}$). To use MSPs for versatile applications, internal and external surfaces of MSPs can be functionalized by various methods. For example, addition of magnetic cores to allow targeting of nanoparticles under magnetic force, and binding cancer specific ligands to the surface of MSPs have been applied [14,15].

Taken together, the objective of the present study is to suggest a delivery system for DSF, and the investigation of the chemotherapeutic effect of DSF combined with copper (Cu^{2+}) and/or sodium nitroprusside (SNP) on breast cancer (Fig. 1). First, magnetic nanoparticles (Fe_3O_4 MNPs) were fabricated as a core material due to their ability to move under a permanent magnetic field. The Fe_3O_4 MNPs were coated with mesoporous silica ($\text{Fe}_3\text{O}_4@\text{mSiO}_2$) to achieve MNPs that are biocompatible, water dispersible and have a large surface area. After DSF loading to the $\text{Fe}_3\text{O}_4@\text{mSiO}_2$ MNPs, folic acid conjugated polyethyleneimine (PEI-FA) was used for encapsulation of DSF-loaded MNPs ($\text{Fe}_3\text{O}_4@\text{mSiO}_2\text{-DSF@PEI-FA}$, mMDPF) to increase both the dispersibility of drug-loaded MNPs in water and the selective cellular

uptake of NPs by cancer cells. The in vitro effect of the mMDPF has also been investigated in the presence of Cu^{2+} and/or SNP on both non-tumorigenic (MCF-10A) and tumorigenic (MCF-7) cells.

2. Materials and methods

2.1. Synthesis of nanoparticles ($\text{Fe}_3\text{O}_4@\text{mSiO}_2$)

Fe_3O_4 MNPs with high crystalline structure were synthesized by thermal decomposition according to the literature [16]. In a typical synthesis, 3 mmol of $\text{Fe}(\text{acac})_3$ (Sigma) was dissolved in 15 mL of benzyl ether (Sigma) and 15 mL of oleylamine (Sigma). The solution was dehydrated at $110 \text{ }^\circ\text{C}$ for 1 h under inert atmosphere, then quickly heated to $300 \text{ }^\circ\text{C}$ at a heating rate of $10 \text{ }^\circ\text{C}/\text{min}$ and aged at this temperature for 1 h (PC44-PC77-PC99 and pt-100, ORDEL). After the reaction, the solution was allowed to cool down to room temperature. The Fe_3O_4 MNPs were extracted upon the addition of ethanol, followed by centrifuging at 9000 rpm for 15 min (NÜVE NF1200R). The final Fe_3O_4 MNPs were dispersed in hexane (Sigma) and stored under inert atmosphere.

Magnetic mesoporous silica nanoparticles ($\text{Fe}_3\text{O}_4@\text{mSiO}_2$ MNPs) were synthesized by sol gel reaction according to the literature [17].

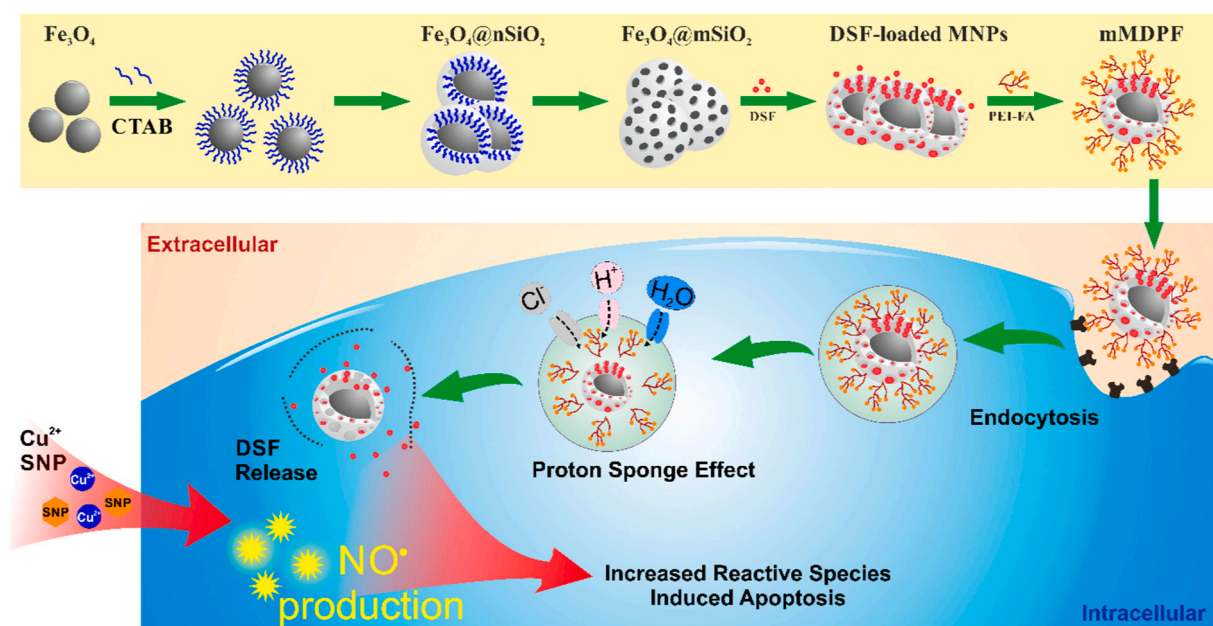


Fig. 1. Schematic illustration of purposed cancer-selective treatment by magnetic mesoporous DSF-loaded nanoparticles. CTAB, cetrimonium bromide; DSF, Disulfiram; PEI-FA, folic acid conjugated polyethyleneimine; mMDPF, $\text{Fe}_3\text{O}_4@\text{mSiO}_2\text{-DSF@PEI-FA}$; Cu^{2+} , copper; SNP, Sodium Nitroprusside; $\text{NO}\cdot$, nitric oxide.

7.5 mg of oleylamine stabilized monodisperse MNPs dispersed in 0.5 mL of chloroform (Sigma) were added to 5 mL of aqueous solution containing 0.1 g of cetrimerium bromide (0.274 mmol CTAB, Fluka). After vigorous stirring of the resulting solution, a homogeneous oil-in-water microemulsion was obtained. Heating at 70 °C for 15 min induced evaporation of the chloroform of the solution, which generated aqueous phase dispersed nanoparticles. Then 0.5 mL of the resulting aqueous solution was diluted with 10 mL of deionized water. Then, 0.3 mL of ammonia solution (2.27 mmol, Sigma), 0.05 mL of TEOS (0.223 mmol, Sigma), and 0.5 mL of ethyl acetate (5.11 mmol, Sigma) were successively added to the diluted aqueous solution containing the MNPs. The resulting mixture was stirred for 30 s, and then aged for 3 h. The precipitate was collected by centrifugation and washed with water and ethanol for 5 times. Finally, the organic materials (CTAB) were removed from the extraction by calcination at 550 °C for 5 h to produce MNPs embedded in mesoporous silica spheres. Fe₃O₄@mSiO₂ MNPs were stored at room temperature after drying.

2.2. Drug loading and surface modification (Fe₃O₄@mSiO₂-DSF@PEI-FA, mMDDPF)

Firstly, 300 mg of folic acid (FA, Sigma) was activated by 93 mg of dicyclohexylcarbodiimide (DCC, Sigma) and 77 mg of N-hydroxysuccinimide (NHS, Sigma) dissolved in dimethylformamide (DMF, Sigma)/dimethyl sulfoxide (DMSO, Sigma) (27 mL, 3:1, v/v) solution with stirring for 24 h according to the literature [14]. Subsequently, the 5% solution of polyethyleneimine (PEI, Sigma) was added to the activated FA solution and allowed to react with stirring overnight at room temperature. Meanwhile, 250 mg of Fe₃O₄@mSiO₂ MNPs were completely dispersed in a 20 mL of disulfiram (DSF, Sigma) solution (0.5 mg of DSF in 25 mL of methanol). The covalently bonded PEI-FA was added into the DSF solution and mixture was stirred for 24 h at room temperature.

The PEI-FA mixture was mixed with Fe₃O₄@mSiO₂-DSF solution and stirred for 2 h (180 rpm). The mixture was centrifuged and washed with water and ethanol several times to obtain Fe₃O₄@mSiO₂-DSF@PEI-FA spheres called mMDDPF. The amount of DSF in mMDDPF was measured by high-performance liquid chromatography (HPLC) and thus drug loading capacity (DLC) was calculated. Characterization of surface modification and loading of the drug were also confirmed by Fourier-transform infrared spectroscopy (FTIR).

2.3. Nanoparticle characterization

X-ray diffraction (XRD) patterns were obtained with D2 Bruker (Physics Department, Faculty of Science, Atatürk University, Erzurum, Turkey) diffractometer (CuKα λ = 1.54 Å). Vertex 70 V FTIR spectrometry (East Anatolia High Technology Application and Research Center (DAYTAM), Atatürk University, Erzurum, Turkey) was used to determine the functional groups on the surface of the nanoparticles. The ζ-potential, hydrodynamic dimensions (R_h) and polydispersity indexes (PDI) of the nanoparticles were measured with a Zetasizer device (ZS90, Malvern, DAYTAM, Atatürk University, Erzurum, Turkey). Transmission electron microscopy (TEM) was performed with a FEI TALOS F200S (Bayburt University, Bayburt, Turkey) by using carbon coated copper grid. The pore distribution and the surface area of the particles were determined using Brunauer-Emmett-Teller (BET) and Barrett-Joyner-Halenda (BJH) methods (Micromeritics 3 Flex, DAYTAM, Atatürk University, Erzurum, Turkey). Folic acid conjugation to PEI was confirmed by UV/NIR spectrophotometry (Shimadzu UV-3600 Plus, DAYTAM, Atatürk University, Erzurum, Turkey), as FA showed absorbance peak at λ = 280–370 nm [18].

2.4. Investigation of drug release kinetic

To investigate DSF release kinetic of mMDDPF, it was incubated in

the buffer (pH 7.4 and pH 6.0) for 4, 6, 7, 8, 18 and 24 h at 37 °C. The amount of residual DSF was analyzed by HPLC (Agilent technology 1260 Infinity II) which consists of an Ace C18 column (5 μm, 250 × 4.6 mm) and UV detector. Water-methanol (20/80, v/v) was used as the mobile phase at a flow rate of 0.7 mL/min. The column temperature was set to 30 °C, the UV detector to 275 nm and the injection volume to 5 μL.

2.5. Cell culture

The ER+ breast tumor cell line (MCF-7) was cultured in Dulbecco's modified Eagle's medium (DMEM, Gibco) containing 1% penicillin-streptomycin (Gibco) and 10% fetal bovine serum (FBS, Gibco) as recommended. The effects of all treatments on cancer cells are compared with non-tumorigenic cell line (MCF-10A) which was cultured in Dulbecco's Modified Eagle Medium/Nutrient Mixture F-12 (DMEM/F12, Gibco) supplemented with 5% horse serum (Gibco), 1% penicillin-streptomycin (Gibco), hydrocortisone (0.5 mg/mL, Sigma), insulin (10 μg/mL, Sigma), epidermal growth factor (EGF, 20 ng/mL, Sigma) and cholera toxin (100 ng/mL, Sigma). Cells were maintained in 90% humidity, 5% CO₂ and at 37 °C (NUAIRE). The cells were photographed with AxioCam ERc 5 s type Zeiss brand camera.

2.6. Cell proliferation and cytotoxicity

The cells were plated at a density of 5000 per well in a 96-well plate, fed with standard media of cell lines and subsequently treated with copper (II) chloride (CuCl₂), DSF, SNP, NPs or their combination. MTS assay (MTS Cell Proliferation Assay Kit (Colorimetric), 197,010, ABCAM) was used to determine the proliferative and cytotoxic effects of the treatments on the cells. 20 μL of MTS solution was added to the cells in the 96-well plates (200 μL) at 24 or 48 h. After 3 h of addition of MTS, the absorbance values at 490 nm were measured with Plate Reader (BioTech). Cell viability (%) was calculated according to the Cell Viability % = (A_{Treatment}/A_{Control}) × 100 formulation. Results are shown as mean ± standard deviation from three independent experiments, each performed in triplicate. Using dose-dependent MTS results, the half maximal inhibitory concentration (IC₅₀) values were calculated in the Origin Pro Lab 8.5 program to compare the effect of treatments on cells.

2.7. Cellular uptake of NPs

Prussian Blue Staining, which is a coloring used to determine the debris in the cell, was applied to investigate cellular uptake of mMDDPF NPs [19]. To this end, 50,000 cells were seeded in 12 well culture dishes with 1 mL of medium, and the culture dishes were incubated for 24 h. After adding 0.5 mg/mL of mMDDPF to the cells, the culture dishes were placed on the top of a magnet for 10 min for one group. After 24 h incubation, cells were washed 3 times with ice cold phosphate-buffered saline (PBS). The cells were then fixed with 4% paraformaldehyde for 20 min at room temperature. Cells were incubated with freshly prepared Prussian Blue solution (1:1 v/v, 20% aqueous hydrochloric acid solution and 10% potassium ferrocyanide solution) for 30 min at 37 °C. Cells were washed with PBS and observed with an inverted microscope.

2.8. Colony-formation assay

Clonogenic assay is a cytotoxicity assay used to investigate the reproductive and colony forming capacities of cells. First, cells were seeded in 12-well plates at 50,000 cells/well and exposed with desired amount of mMDDPF, Cu and/or SNP. After 24 h incubation [6], cells were harvested. Cells were re-cultured with fresh medium containing no drug as 50 cells/well. At least 50 cells were counted as clonogenic cells after 7–10 day [5,6]. Cells were washed with PBS, fixed with cold methanol. Colonies were visualized with 10% trypan blue solution in

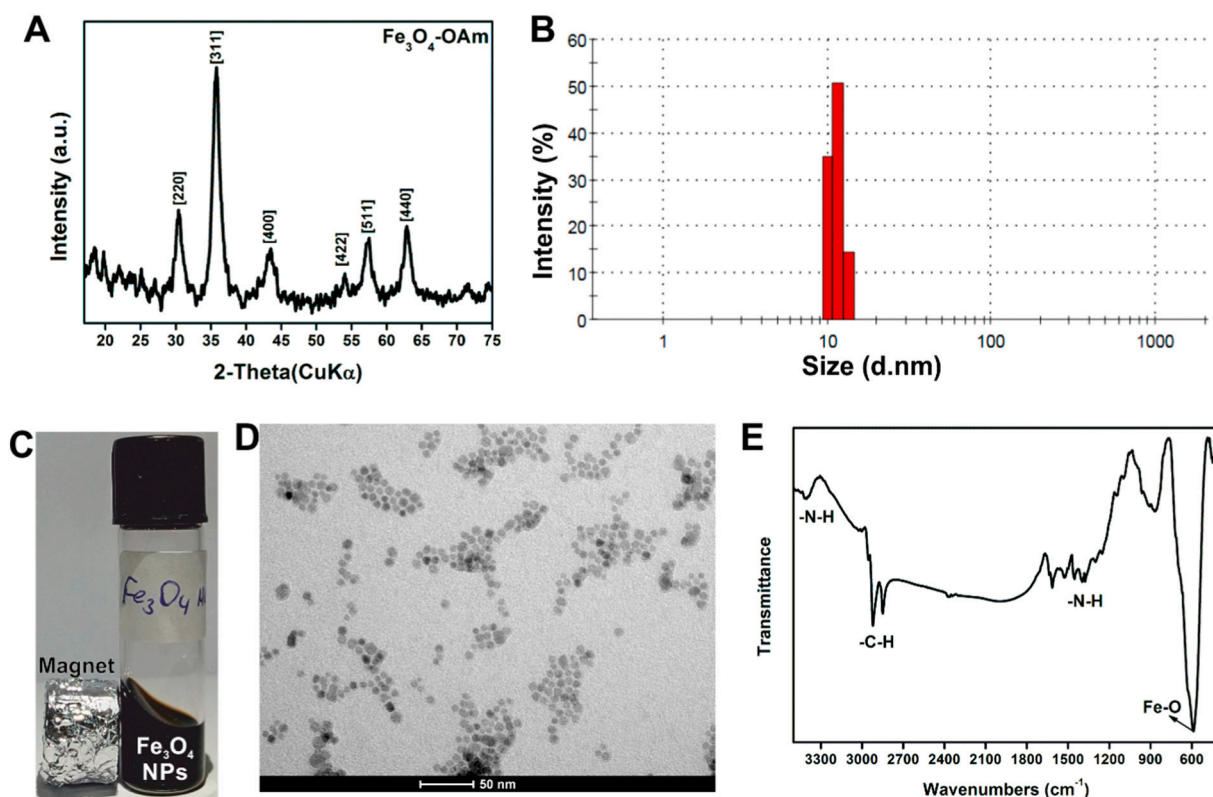


Fig. 2. Characterization of nanoparticles. A. XRD pattern, B. distribution of hydrodynamic size, C. magnetic response, D. TEM image and E. FTIR spectrum of oleylamine-stabilized Fe_3O_4 MNPs.

PBS and counted.

2.9. Statistics

All results were analyzed with Origin Pro Lab 8.5 data analysis and graphing software. Statistical comparisons were made using one-way ANOVA (Analysis of variance) with post hoc comparison (Tukey test). Statistical significance was considered when $p < 0.05$ and $p < 0.001$ ($n = 3$).

3. Results and discussion

3.1. Magnetic mesoporous silica nanoparticles with large surface areas

The oleylamine-stabilized iron oxide magnetic core (Fe_3O_4 MNPs) were synthesized by a high-temperature organic phase decomposition method which uses $\text{Fe}(\text{acac})_3$ as an iron precursor because of its low cost and high yield. Fig. 2A demonstrates that the Fe_3O_4 MNPs are single crystal and the XRD peaks of at 30.27 , 35.68 , 37.43 , 43.01 , 54.17 , 57.56 and 62.97° represent the inverted cubic spinel magnetite [220], [311], [222], [400], [422], [511] and [440] respectively [20,21]. Hydrodynamic size (R_h) measurement (Fig. 2B) showed that the Fe_3O_4 MNPs smaller than 15 nm with a narrow size distribution (less than 5% standard deviation). According to the magnetic responsiveness image of Fe_3O_4 MNPs in Fig. 2C, MNPs have great movement towards the magnet. TEM images were also consistent with the result of R_h measurement, indicating that the MNPs were hexagonal in shape, monodisperse and have an average 10 nm size (Fig. 2D). The $-\text{NH}_2$ group of oleylamine was observed at 3412 , 1577 and 1330 – 1650 cm^{-1} peaks in the FTIR spectrum which is presented in Fig. 2E [22]. The absorption bands at 3014 , 2920 and 2850 cm^{-1} show C–H vibrations of the $-\text{CH}_2$ and $-\text{CH}_3$ groups present in the oleylamine [16,22]. The peaks at 1455 and 1400 cm^{-1} show vibrations originating from

asymmetric and symmetric $-\text{CH}_3$. The strong absorption of the oxygen complex with the octahedral iron in the Fe_3O_4 MNPs was observed at the peak at 588 cm^{-1} [16,23]. Correspondingly, the peak at 447 cm^{-1} may indicate Fe–O deformation [16]. These findings indicate that oleylamine-stabilized magnetite was synthesized successfully.

The amine group of oleylamine interacts weakly with Fe_3O_4 MNP's surface and is easily removed from the surface of the particle in the presence of chloroform [20,24,25]. The Fe_3O_4 MNPs were coated with silica to obtain non-porous core/shell NPs ($\text{Fe}_3\text{O}_4@n\text{SiO}_2$) by the sol-gel method in the presence of a bipolar surfactant, cetrimonium bromide (CTAB). Thus, the transition of the particles from the organic phase to the water phase is ensured by mixing chloroform solution with CTAB aqueous solution and Van der Waals interaction takes place between the CTAB and the Fe_3O_4 MNPs instead of oleylamine [24,25]. Silica-coated MNPs were produced using CTAB-stabilized nanoparticles as seeds. Structural and morphological analysis revealed that the non-porous $\text{Fe}_3\text{O}_4@n\text{SiO}_2$ MNPs were monodisperse, spherical and less than 100 nm according to SEM images as shown in Fig. 3A. Mesoporous core/shell NPs ($\text{Fe}_3\text{O}_4@m\text{SiO}_2$) were obtained by removing CTAB from the $\text{Fe}_3\text{O}_4@n\text{SiO}_2$ MNPs and characterized by TEM, presented in Fig. 3B. To determine the surface area, pore volume and pore size of the $\text{Fe}_3\text{O}_4@m\text{SiO}_2$ MNPs, the nitrogen adsorption-desorption technique was used. The nitrogen sorption isotherms show typical type IV according to the IUPAC (International Union of Pure and Applied Chemistry) classification with a H4 hysteresis loop which is a typical characteristic of mesoporous materials with hexagonal cylindrical channels and open pores with bottle neck entrances [12]. The surface area of the $\text{Fe}_3\text{O}_4@m\text{SiO}_2$ MNPs is $930.38 \text{ m}^2/\text{g}$ (Fig. 3C) while the surface area of $\text{Fe}_3\text{O}_4@n\text{SiO}_2$ MNPs is $44.40 \text{ m}^2/\text{g}$ (data not shown), that means the surface area of NPs increased almost 20 times after calcination. The result of the BJH makes evident that uniform $\text{Fe}_3\text{O}_4@m\text{SiO}_2$ MNPs were produced with a pore volume of $0.73 \text{ cm}^3/\text{g}$ and a pore diameter of 2.74 nm (Fig. 3C). The narrow peak (peak center at

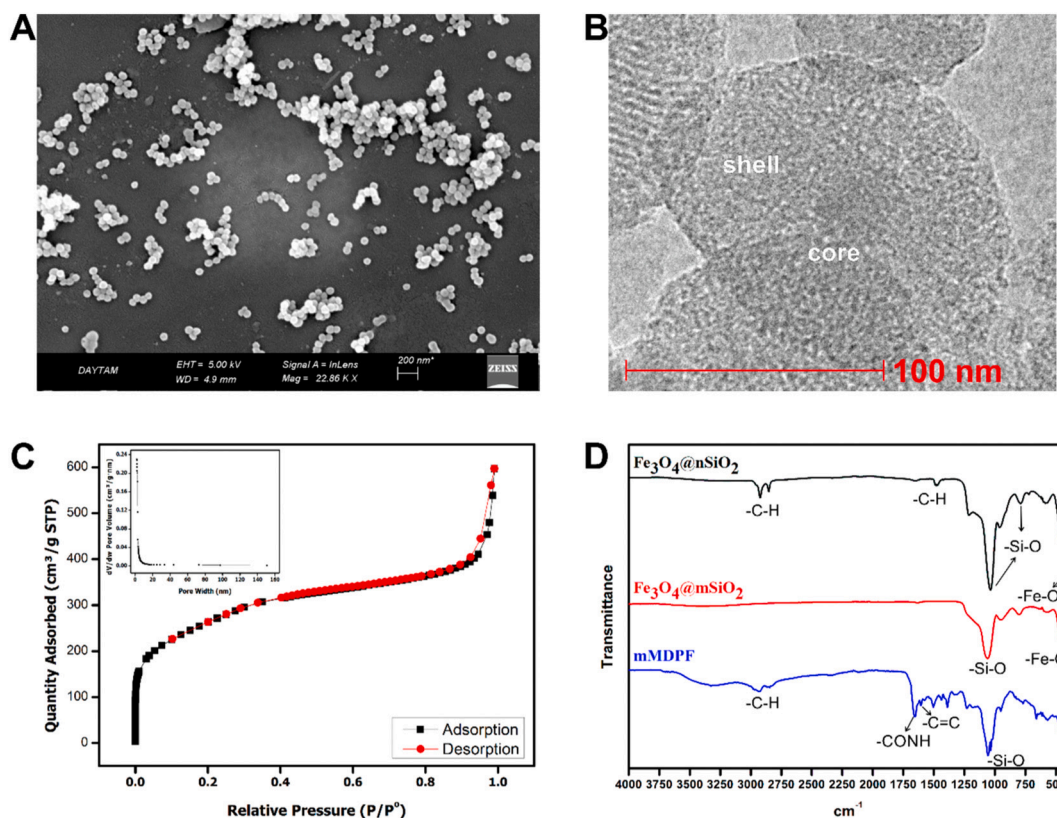


Fig. 3. Characterization of nanoparticles. A. SEM image of Fe₃O₄@mSiO₂ MNPs, B. TEM image of folic acid-functionalized polyethyleneimine-coated disulfiram-loaded MNPs (mMDPF), C. BET-BJH results of Fe₃O₄@mSiO₂ MNPs and D. FTIR results of non-porous (Fe₃O₄@nSiO₂), porous (Fe₃O₄@mSiO₂) and mMDPF.

about 2 nm) observed in the pore size graph shows that uniform and narrow pore structures are obtained. Although there is a very high temperature in the calcination process, there is no significant difference in inorganic groups according to the FTIR spectrum (Fig. 3D). These results fit with previous studies [26]. However, calcination reduces the toxicity of Fe₃O₄@SiO₂ MNPs by causing reduced silanol groups which are responsible for cytotoxicity [27]. In Fig. 3D, the absorption of -OH, which facilitates silica-coated particles being well dispersed in water, appears to be a slightly broad peak at ~3400 cm⁻¹. The peaks seen at 962 cm⁻¹ and around 1630 cm⁻¹ indicate that the particles have hydrophilic silanol (-Si-OH) on the surface [28,29]. The peaks at 1221 and 1041 cm⁻¹ to 788 cm⁻¹ and 433 cm⁻¹ belong symmetric and asymmetric -Si-O- bonds [28,30]. Furthermore, complete removal of CTAB ensures both regular pore structures and is necessary to reduce the cytotoxic effect of the delivery system [31]. Based on the FTIR results, the disappearance of the peaks at 2923 and 2855 cm⁻¹ demonstrates that the CTAB molecule is successfully removed [32]. All these findings increase the ideal characteristics of the prepared drug delivery system.

3.2. Drug loading to targeted magnetic nanocarrier system (mMDPF) and drug release

Following preparation of the mesoporous core/shell Fe₃O₄@mSiO₂ MNPs, DSF was loaded into the pores. In this study, it was determined that DSF is stable in methanol for 3 months. Some researchers have used DMSO as a solvent in the DSF loading process, but this has led to a decrease in drug encapsulation rate during dialysis to remove cytotoxic DMSO [33]. Therefore, the DSF loading process to the Fe₃O₄@mSiO₂ MNPs was maintained in methanol. The DSF in methanol was mixed with the Fe₃O₄@mSiO₂ MNPs for 24 h at room temperature. In the case of residual methanol in the structure, the cytotoxicity of Fe₃O₄@mSiO₂ MNPs without DSF was also investigated. The weak interactions between the DSF and the silica are established, whereby the hydrophobic

DSF is located in the hydrophobic pores during loading (Fig. S1).

Subsequently, the DSF-loaded Fe₃O₄@mSiO₂ MNPs were coated with polyethyleneimine-folic acid (PEI-FA). Positively charged PEI provides positive charge to the surface of NPs, increases the dispersion of the MNPs in water, and ensures safe transportation of the cargo to the target tissues/cells [34]. Another advantage of PEI is that the effective transport of cargo to the cytoplasm (endosomal escape) by the proton sponge effect because of its high pH-buffering capacity [35]. The reason for the use of FA as a targeting agent is that most of the cancer cells, especially metastatic species, overexpress the FA receptor [36]. Therefore, FA conjugation to nanoparticle surfaces increases the cellular uptake of the nanoparticles by cancer cells. The PEI-FA was prepared by the amidation reaction between the amide groups of PEI and the carboxyl groups of FA before adding into the solution of DSF-loaded or DSF-free nanoparticles [37]. The newly established amide bond was observed at 1660 cm⁻¹ in the IR spectrum (Fig. 3D). The drug-loaded NPs were encapsulated with the PEI-FA and called mMDPF (Fe₃O₄@mSiO₂-DSF@PEI-FA) while DSF-free nanoparticles were called mMPF (Fe₃O₄@mSiO₂@PEI-FA). The surface modification with PEI-FA was caused a decrease in the -Si-O- and -Si-OH peaks observed in the FTIR spectrum [38]. The peaks at 3324 and 1504 cm⁻¹ indicate the -NH deformation in the PEI structure. The C-H vibrations of PEI were observed at 2846 and 1107 cm⁻¹. The aromatic C=C and phenyl ring of the folic acid (FA) structure caused peaks at 1606 cm⁻¹ and 1488 cm⁻¹, respectively. The hydrodynamic diameter (R_h) of prepared mMDPFs is ~160 nm as stated by DLS results (Fig. 4A) which is within the agreeable size range for drug delivery, because the size of drug delivery systems must be less than 200 nm for higher cellular uptake [39]. The presence of FA was also confirmed with the UV spectroscopy. Absorption peaks of FA at λ = 280 nm and λ = 360 nm were observed in the mMDPFs unlike Fe₃O₄@mSiO₂ MNPs as seen in Fig. 4B [14,15,18,37]. Thus, consistent with FTIR results, FA modification was confirmed to be successful.

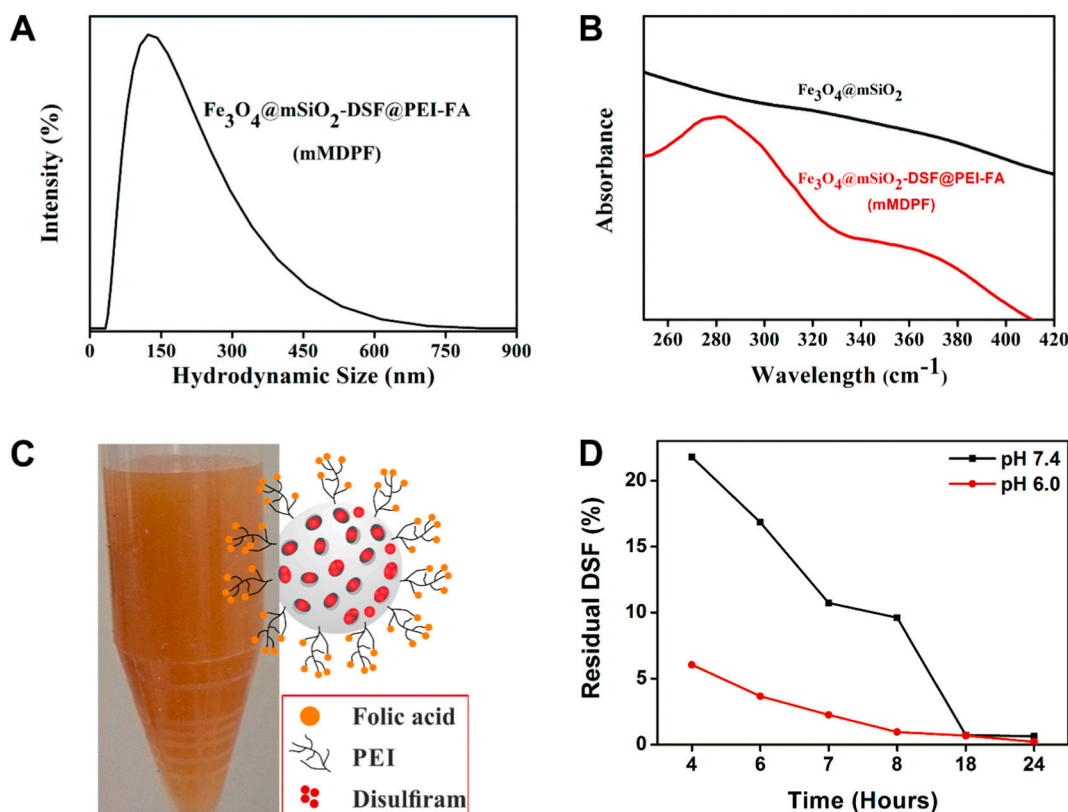


Fig. 4. A. Hydrodynamic diameter of mMDPF, B. UV spectrum of $\text{Fe}_3\text{O}_4@m\text{SiO}_2$ and $\text{Fe}_3\text{O}_4@m\text{SiO}_2\text{-DSF@PEI-FA}$ (mMDPF). C. Picture of mMDPF dispersion in water and D. Residual DSF in mMDPF after incubation at 37°C in the buffers (pH 7.4 and pH 6.0).

mMDPFs was stable and well-dispersed in water (Fig. 4C). The amount of DSF in the mMDPF was elucidated by the HPLC method and calculated from a standard graph (0–30 ppm DSF in methanol). In this study, the loading rate is $43.58 \pm 13.02 \mu\text{g DSF/mg particle}$. As for the issue of drug release, time dependent DSF releasing measurement was applied at 37°C for pH 7.4 and pH 6.0 in PBS buffer. It is not possible to describe the releasing profile of DSF in PBS due to the rapid hydrolysis of DSF in water. So, residual DSF in mMDPFs was measured by HPLC that showed DSF releasing rate was around 90.1% at pH 6.0 in 4 h (Fig. 4D) which is fine to reach therapeutic concentrations into the cytoplasm. Slower DSF release was observed at 37°C and pH 7.4 and the DSF release rate was determined as 64.34% for 4 h (Fig. 4D). DSF is completely released within 24 h-incubation. Faster drug release in the acidic environment suggests that PEI acts as a gate and causes controlled drug release. The fast release of DSF may assure a high accumulation of DSF and rapid inactivation of P-glycoprotein which is responsible for drug resistance and induces apoptosis [10]. Furthermore, magnets accelerate cellular uptake of mMDPFs, which supports fast drug delivery to cancer cells.

3.3. Cancer-specific cytotoxicity and cellular uptake

The aim of this study was selectively increasing the RS concentration in MCF-7 cells to selectively kill cancer cells. DSF is an alcohol-aversion drug that has recently increased interest for cancer treatment. DSF either alone or in synergy with an anticancer agent induces apoptosis in chemotherapy-resistant cells, especially cancer stem cells [4,40]. However, DSF is not stable in blood, acidic or copper-rich environments. Therefore, DSF must be delivered to target tissues by a drug carrier system. There are various studies about targeting delivery of DSF [41–43]. For the first time, in this study, magnetic mesoporous nanoparticles were used for DSF delivery. Here, DSF is a main RS generator. Cu^{2+} and SNP were also used to increase the effect and

selectivity of DSF onto the MCF-7 cells. Firstly, different concentrations of DSF, Cu^{2+} and SNP were applied to MCF-7 and MCF-10A cells, and their toxic effects were determined separately. Fig. 5 shows the cell viability of MCF-7 and MCF-10A exposed to DSF (0–10 μM), Cu^{2+} (0–10 μM) and SNP (0–10 mM). The IC_{50} value was calculated for DSF exposed cells. The IC_{50} value of DSF was found to be 5.33 μM for MCF-7 cells and 17.80 μM for MCF-10A cells at the end of the 24-h incubation. Song et al. reported that the IC_{50} of DSF was 18 μM after 48 h for MCF-7 cells [44]. Wiggins et al. found that IC_{50} of DSF was 0.3 μM for MCF-7 cells and $> 10 \mu\text{M}$ for MCF-10A cells [24].

In this study, ~60% of cell viability was observed for 0.5 μM DSF treated cancer cells (MCF-7) at 48 h. Faasehee et al. reported the cell viability as 68% for 24th h of 0.5 μM DSF-treated MCF-7 cells [33]. As can be seen from Fig. 5B, the proliferation of non-tumorigenic cells (MCF-10A) is 97% for 10 μM DSF at 48 h. It can be concluded that MCF-7 is more sensitive to disulfiram than MCF-10A at range of 0.1–10 μM concentrations (Fig. 5A, B). However, cell viabilities were not dependent to DSF concentration at range of 0.5–10 μM disulfiram. The cancer cells may be protected at relatively higher concentration of DSF.

MCF-7 and MCF-10A cells were incubated with 0.1–10 μM Cu^{2+} containing media and no serious cell death was observed (Fig. 5C, D). MCF-7 cells were slightly more sensitive to Cu^{2+} than MCF-10A. It was observed that cell growth was encouraged in the 48-h incubation of Cu^{2+} -treated MCF-7 cells at low concentrations. In groups treated with Cu^{2+} at a concentration of 10 μM , a statistically significant difference (< 0.05) was observed after 48 h, but no significant difference was observed for other concentrations. Therefore, 5 μM was preferred in Cu^{2+} applications.

The MTS results of SNP treatment demonstrated that 0.1–1 mM of SNP treatment might selectively decrease cancer cell viability at the 48th-hour incubation, but 5 and 10 mM of SNP killed 90% of both cell lines (Fig. 5E, F). It was observed that all the groups treated with SNP were statistically different from the control group (< 0.05). On the

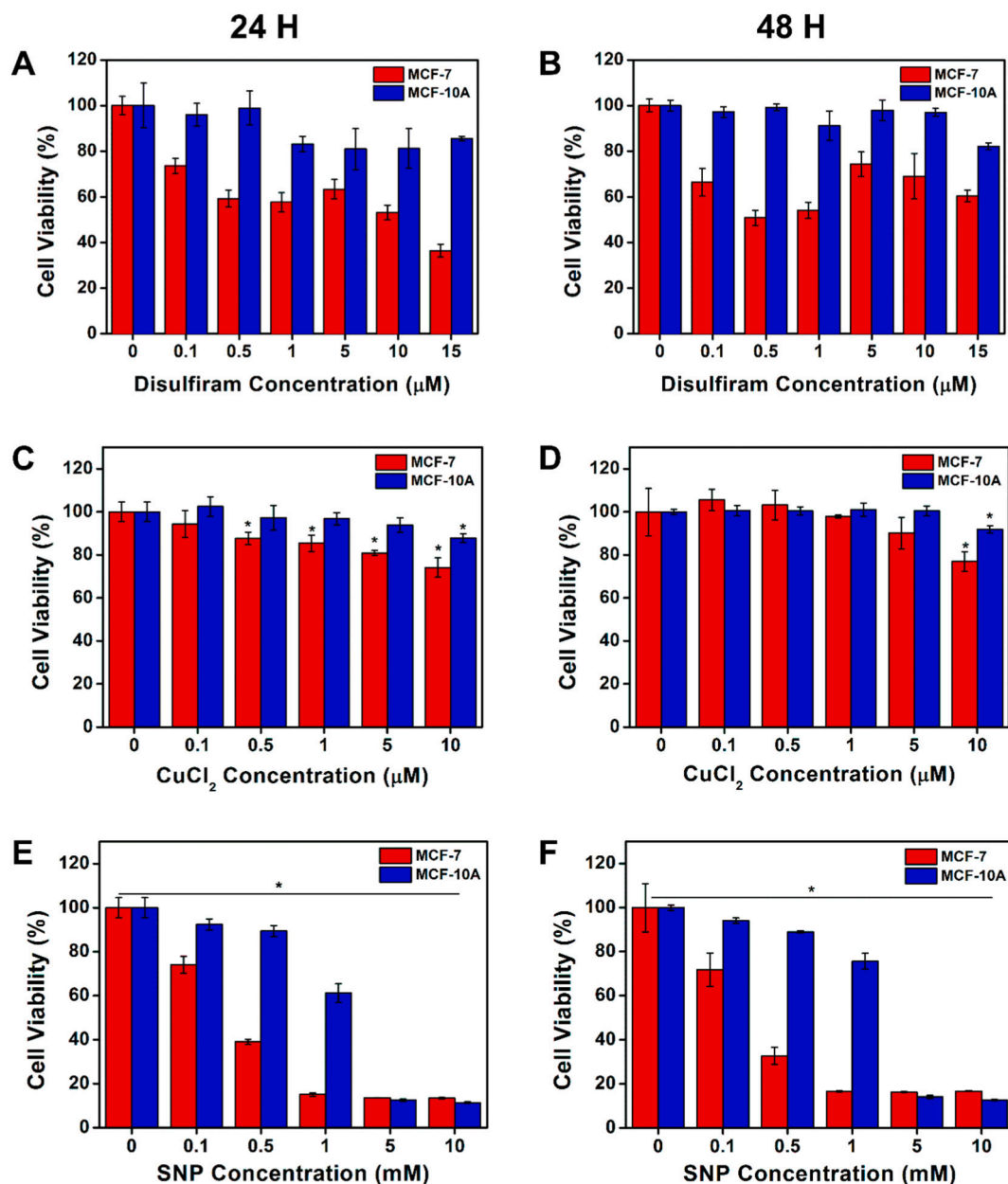


Fig. 5. MTS cytotoxicity results on MCF-7 and MCF-10 cells treated with DSF (0.1–10 μM), CuCl_2 (0.1–10 μM) and SNP (0.1–10 mM) for 24 (A., C. and E.) and 48 (B., D. and F.) hours. $p < 0.05$ DSF, Disulfiram; Cu^{2+} , copper; SNP, Sodium Nitroprusside. *: $p < 0.05$.

other hand, no statistically significant difference was found between the groups treated with 0.1 and 0.5 mM of SNP in MCF10A cells. Therefore, SNP concentration was used as 0.5 mM in ongoing studies. In this manner, the cell selectivity of DSF, Cu^{+2} or SNP has been shown to be concentration-dependent.

Studies with mesoporous silica nanoparticles (MSPs) have revealed that the toxic effect of MSPs is different with respect to the cell type and generally shows toxicity above 100 $\mu\text{g}/\text{mL}$ [27,45]. Similarly, in this study, mMPF ($\text{Fe}_3\text{O}_4@/\text{mSiO}_2@/\text{PEI-FA}$) caused limited cell death for both of the cells (Fig. 6) at lower concentrations, consistent with the previous results [46]. MCF-7 has been observed to be slightly more sensitive to mMPF than MCF-10A. This situation can be interpreted as cellular uptake of mMPF by MCF-7 cells is higher as a result of folic acid (FA) surface modification performed due to the fact that MCF-7 cells contain more FA receptors than MCF-10A [47].

DSF-loaded mMPFs ($\text{Fe}_3\text{O}_4@/\text{mSiO}_2\text{-DSF@PEI-FA}$, mMDPF) at 60, 80 and 100 $\mu\text{g}/\text{mL}$ concentration effectively destroyed MCF-7 cells after

48 h. However, MCF-10A cells show high proliferation at the same concentrations of mMDPF (Fig. 6A, B). As a result, it can be said that the targeted delivery of DSF dramatically increases selective cancer cell death. Cell medium was examined with a microscope after mMDPF was applied for 72 h and it was observed that the MCF-7 media contained fewer MNP aggregates than the MCF-10A medium (Fig. 6C). On the other hand, Prussian Blue dye is used to detect the presence of iron nanoparticles in cells. mMDPF contains an iron core and Prussian Blue gives blue color in the presence of iron. As can be seen from Fig. 6D, blue zones appear in MCF-7 cells with mMDPF while MCF-10A cells do not remarkably contain blue zones. As a result, it can be said that mMDPF cellular uptake is higher in MCF-7 cells compared to MCF-10A cells.

3.4. Combine therapy induces selective tumor cell death

DSF is converted to diethyldithiocarbamate (DDC) in the cytoplasm

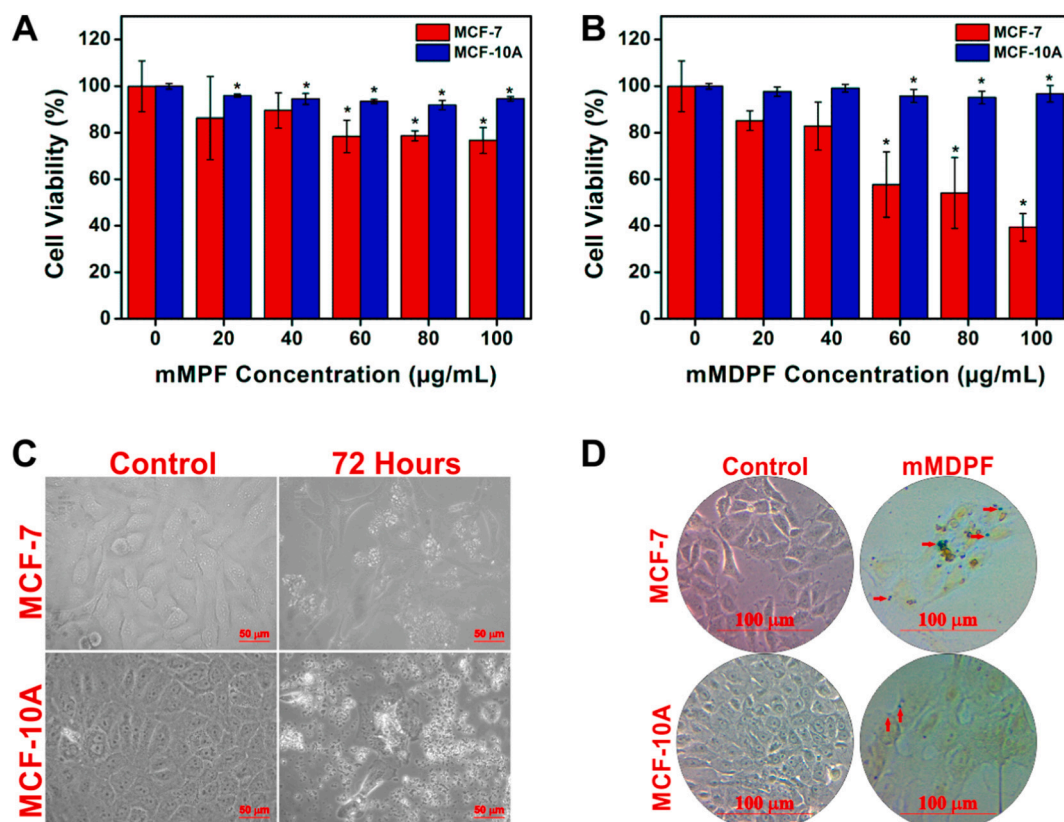
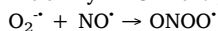


Fig. 6. MTS cytotoxicity results on MCF-7 and MCF-10 cells treated with A. mMPF (20–100 µg/mL) and B. mMDPF (20–100 µg/mL) for 48 h, C. Microscope images of mMDPF-treated cells for 72 h and D. Cells were exposed to 500 µg/mL of mMDPF before the Prussian Blue staining (red arrows). mMDPF, Fe₃O₄@mSiO₂-DSF@PEI-FA; mMPF, Fe₃O₄@mSiO₂@PEI-FA. *: $p < 0.05$. (For interpretation of the references to color in this figure legend, the reader is referred to the web version of this article.)

[48]. DDC is much more unstable than DSF and is rapidly broken down into CS₂ and dialkylamine. DDC inhibits a variety of enzymes including SOD due to its affinity for sulfhydryl groups and the ability to bind the copper and zinc of SOD [49]. SOD inhibition can cause superoxide accumulation in the cells. Therefore, DSF can be used as an RS generating cancer drug. Hyeon-Yeol et al. showed that DDC loaded NPs increase reactive species in cancer cells [50].

The RS generating effect of DSF may be increased by the addition of transition metals. For example, DDC-Cu complex has a great therapeutic effect on cancer via producing RS and causing rapid cell death [51]. Cu²⁺ is also a necessary cofactor for tumor growth, invasion and metastasis, and it is quite plausible to use Cu²⁺ chelating agents such as DSF in the treatment of cancer. Interestingly, Cu²⁺ addition increases the therapeutic effect of DSF in different cancer cell types [4,5,52]. Therefore, in this study, the synergistic effect of Cu²⁺ (5 µM) and DSF was tested (Fig. 7A).

As mentioned above, DSF inhibits SOD and causes O₂^{•-} accumulation. An irreversible reaction between NO[•] and O₂^{•-} generates peroxynitrite (ONOO[•]) which is a RS. Hyeon-Yeol et al. showed that SOD inhibition by DDC in the presence of NO[•] generates ONOO[•] [50].



Therefore, DSF + NO[•] may increase RS based damage to cancer cells. In addition, it has been reported that SNP elevates the intracellular levels of reactive oxygen species or decreases the cytotoxic effect of DDC-Cu complexes, depending on concentration [53,54]. However, NO[•] is an unstable molecule and thus it has to be generated by NO[•] generator molecules in the cells. In this study, for this purpose, SNP was used. SNP is an FDA (U.S. Food and Drug Administration)-approved NO[•] donor that spontaneously releases NO[•] in the body.

To evaluate synergistic effects, the MCF-7 and MCF-10A cells were incubated in a mixture of DSF (1 µM), Cu²⁺ (5 µM) and SNP (0.5 mM)

for 24 h. Fig. 7A shows that the combination of non-targeted DSF with Cu²⁺ and SNP slightly induces cancer cell death. The MCF-7 and MCF-10A were also exposed to mMPFs (60 µg/mL) in the mixture of Cu²⁺ (5 µM) and SNP (0.5 mM) for 24 h. mMPF did not contain DSF and the effectiveness of the combination therapy (Fig. 7B) was similar to Fig. 6. It is well understood that the Cu²⁺ (5 µM) or SNP (0.5 mM) treatment without targeted DSF is not effective on both MCF-7 and MCF-10A cells. However, targeted delivery of DSF (60 µg/mL of mMDPFs) with Cu²⁺ (5 µM) and SNP (0.5 mM) dramatically increased selective cancer cell death for 24 h (Fig. 7C).

For targeting, in addition to folic acid conjugation on the surface of NPs, the magnetic property of the mMDPFs was used. After the treatment of the cells with mMDPFs, the magnet was retained on the bottom surface of the cell culture dish. Thus, cellular uptake of mMDPFs was accelerated and drug release was mainly maintained in the cell.

Cancer cells as their nature, tend to form colonies, unlike healthy cells. It is desirable that the treatment applied targets the ability of colony formation of cancer cells. MCF-7 and MCF-10A cells were treated with DSF, mMPF and mMDPF, either separately or together with Cu and SNP, to investigate the reproductive and colony ability of the cells. After waiting 12 h for cellular uptake, the cells were re-incubated with fresh medium. After approximately ten days, it was observed that the colony forms of MCF-7 cells were more spherical and distinctive, but MCF-10A cells spread on the surface and proliferated (Fig. 7D). This difference observed in the colony formation of two cell lines was also reported in the literature [55]. Colony counts were not performed in MCF-10A cells since they spread over the surface [6,40,56]. As can be seen from the photographs, it is understood from comparison with untreated control MCF-7 cells, the colony formation ability of mMDPF-treated MCF-7 cells did not change. It is known that DSF + Cu²⁺ application decreases the radius of colony forms and the

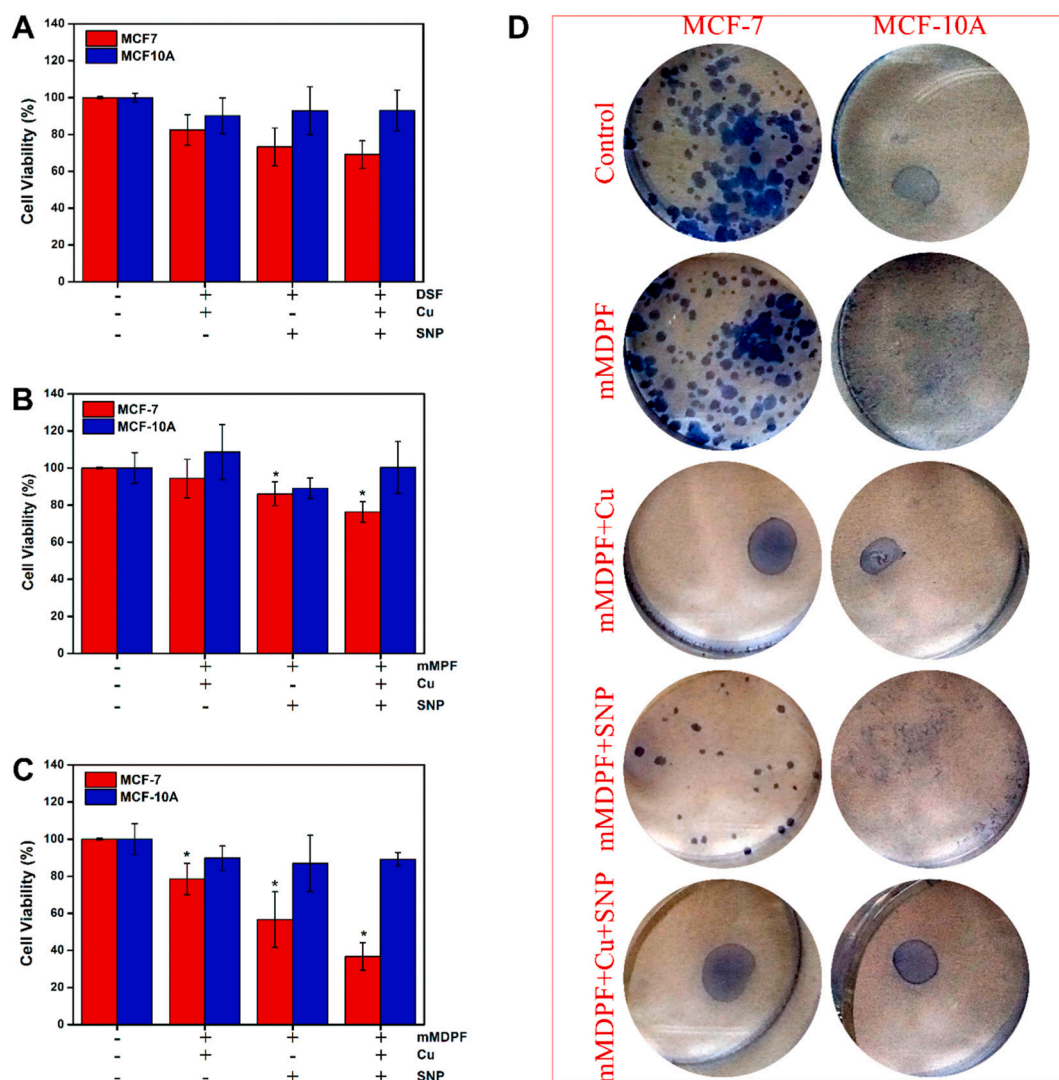


Fig. 7. Cytotoxicity assays for combination therapy. A. DSF (1 μ M), CuCl_2 (5 μ M) and SNP (0.5 mM) treatment. B. mMMPF (60 μ g/mL), CuCl_2 (5 μ M) and SNP (0.5 mM) treatment. C. mMMPF (60 μ g/mL), CuCl_2 (5 μ M) and SNP (0.5 mM) treatment and D. Clonogenic assay results on MCF-7 and MCF-10 cells which are treated with DSF (1 μ M), CuCl_2 (5 μ M), SNP (0.5 mM), mMMPF (60 μ g/mL) and mMMPF (60 μ g/mL) for 24 h. DSF, Disulfiram; mMMPF, Fe_3O_4 @mSiO₂-DSF@PEI-FA; mMMPF, Fe_3O_4 @mSiO₂@PEI-FA; Cu^{2+} , copper; SNP, Sodium Nitroprusside. *: $p < 0.05$.

number of colonies in cancer cells [57,58]. When the groups in which DSF was applied with Cu^{2+} and SNP were compared, it was observed that DSF increased cell death in the presence of Cu^{2+} . DSF + SNP application affected the colony ability of cancer cells less than DSF + Cu^{2+} group. DSF + SNP application did not show an important effect on MCF-10A cells. As a result, in the clonogenic experiment for DSF, the most affected group in MCF-7 cells was observed in DSF + Cu^{2+} + SNP triple application, while this application showed limited effect in MCF-10A cells.

Related to the MTS assay, the colony formation assay results also indicated that Cu^{2+} is essential for anticancer activity of DSF and high concentration of SNP induce cytotoxicity instead of counteracting the DDC-Cu complex toxicity (Fig. 7D). The suggested combination therapy showed potent activity against ER+ breast cancer cell. It is concluded that DSF and Cu^{2+} may decrease cell proliferation by increasing intracellular copper uptake. While DSF induced SOD inhibition may increase the intracellular superoxide level, SNP-induced $\text{NO}\cdot$ release may cause increased oxidative stress as a result of superoxide and $\text{NO}\cdot$ interaction. The Cu^{2+} can modulate the therapeutic potential of a $\text{NO}\cdot$ donor reacting with $\text{NO}\cdot$ [59]. A previous study had shown that the SNP-induced growth of MCF-7 cells is extremely suppressed in the

presence of CuCl_2 (5 μ M) [59]. The production of nitric oxide is decreased by treatment with low concentrations of DDC-Cu complex [54].

4. Conclusion

Drug delivery systems increase the potential of drugs in treatments due to protection of the drug from rapid early degradation. Non-toxic magnetic mesoporous silica nanoparticles have been used for targeting and controllable release of drugs. In this study, DSF-loaded nanoparticles (60 μ g/mL) were used against breast cancer and the treatment was combined with Cu^{2+} (5 μ M) and SNP (0.5 mM). It was observed that the designed nanoparticles selectively killed breast cancer cells (MCF-7). SNP was used as a donor of $\text{NO}\cdot$ that may cause direct damage to membranes, proteins and DNA or stress-induced apoptosis. DSF acted as a SOD inhibitor and broke the modulation of redox adaptation mechanisms and made possible the accumulation of superoxide. Induction of oxidative stress and apoptosis could be triggered with the $\text{NO}\cdot$ interaction with superoxide. Also, Cu^{2+} increased the cytotoxicity of DSF. The triple therapy of DSF, Cu, and SNP may cause high oxidative stresses due to increased intracellular reactive species such as $\text{NO}\cdot$, O_2^- , peroxynitrite, inhibition of proteasomes and NF- κ B inactivation,

and increased intracellular copper content. Future experiments can reveal the mechanism of this suggested combination treatment.

CRedit authorship contribution statement

Kübra Solak: Methodology, Validation, Formal analysis, Investigation, Writing - original draft, Writing - review & editing, Visualization. **Ahmet Mavi:** Conceptualization, Methodology, Validation, Formal analysis, Investigation, Writing - original draft, Writing - review & editing, Funding acquisition. **Bilal Yilmaz:** Formal analysis, Investigation.

Declaration of competing interest

The authors declare that they have no known competing financial interests or personal relationships that could have appeared to influence the work reported in this paper.

Acknowledgment

This work has been supported by Atatürk University (Erzurum, Turkey), Scientific Research Projects Units (BAP- 2015.412 and BAP-2015.202). The authors would like to acknowledge East Anatolia High Technology Application and Research Center (DAYTAM, Erzurum, Turkey) for laboratory support. The authors would like to thank Dr. Abdelbasset Chafik for the corrections and recommendations in the article.

References

- [1] M.-Y. Liou, P. Storz, Reactive oxygen species in cancer, *Free Radic Res* 44 (2010), <https://doi.org/10.3109/10715761003667554>. *Reactive*.
- [2] V. Koppaka, D.C. Thompson, Y. Chen, M. Ellermann, K.C. Nicolaou, R.O. Juvonen, D. Petersen, R.A. Deitrich, T.D. Hurley, V. Vasilou, Aldehyde dehydrogenase inhibitors: a comprehensive review of the pharmacology, mechanism of action, substrate specificity, and clinical application, *Pharmacol. Rev.* 64 (2012) 520–539, <https://doi.org/10.1124/pr.111.005538>.
- [3] B. Cvek, Z. Dvorak, The value of proteasome inhibition in cancer. Can the old drug, disulfiram, have a bright new future as a novel proteasome inhibitor? *Drug Discov. Today* 13 (2008) 716–722, <https://doi.org/10.1016/j.drudis.2008.05.003>.
- [4] X. Guo, B. Xu, S. Pandey, E. Goessl, J. Brown, A.L. Armesilla, J.L. Darling, W. Wang, Disulfiram/copper complex inhibiting NF- κ B activity and potentiating cytotoxic effect of gemcitabine on colon and breast cancer cell lines, *Cancer Lett.* 290 (2010) 104–113, <https://doi.org/10.1016/j.canlet.2009.09.002>.
- [5] X. Liu, L. Wang, W. Cui, X. Yuan, L. Lin, Q. Cao, N. Wang, Y. Li, W. Guo, X. Zhang, C. Wu, J. Yang, Targeting ALDH1A1 by disulfiram/copper complex inhibits non-small cell lung cancer recurrence driven by ALDH-positive cancer stem cells, *Oncotarget* 7 (2016) 58516–58530, <https://doi.org/10.18632/oncotarget.11305>.
- [6] N.C. Yip, I.S. Fombon, P. Liu, S. Brown, V. Kannappan, A.L. Armesilla, B. Xu, J. Cassidy, J.L. Darling, W. Wang, Disulfiram modulated ROS-MAPK and NF κ B pathways and targeted breast cancer cells with cancer stem cell-like properties, *Br. J. Cancer* 104 (2011) 1564–1574, <https://doi.org/10.1038/bjc.2011.126>.
- [7] H. Lövborg, F. Öberg, L. Rickardson, J. Gullbo, P. Nygren, R. Larsson, Inhibition of proteasome activity, nuclear factor- κ B translocation and cell survival by the anti-alcoholism drug disulfiram, *Int. J. Cancer* 118 (2006) 1577–1580, <https://doi.org/10.1002/ijc.21534>.
- [8] Z. Wang, J. Tan, C. McConville, V. Kannappan, P.E. Tawari, J. Brown, J. Ding, A.L. Armesilla, J.M. Irache, Q.-B. Mei, Y. Tan, Y. Liu, W. Jiang, X. Bian, W. Wang, Poly lactic-co-glycolic acid controlled delivery of disulfiram to target liver cancer stem-like cells, *Nanomedicine* (2016) 1–17, <https://doi.org/10.1016/j.nano.2016.08.001>.
- [9] X. Chen, L. Zhang, X. Hu, X. Lin, Y. Zhang, X. Tang, Formulation and preparation of a stable intravenous disulfiram-loaded lipid emulsion, *Eur. J. Lipid Sci. Technol.* 117 (2015) 869–878, <https://doi.org/10.1002/ejlt.201400278>.
- [10] X. Duan, J. Xiao, Q. Yin, Z. Zhang, H. Yu, S. Mao, Y. Li, Smart pH-sensitive and temporal-controlled polymeric micelles for effective combination therapy of doxorubicin and disulfiram, *ACS Nano* 7 (2013) 5858–5869, <https://doi.org/10.1021/nn4010796>.
- [11] H. Huang, J.F. Lovell, Advanced functional nanomaterials for theranostics, *Adv. Funct. Mater.* 27 (2017), <https://doi.org/10.1002/adfm.201603524>.
- [12] Z.A. Allothman, A review: fundamental aspects of silicate, *Materials (Basel)* 5 (2012), <https://doi.org/10.3390/ma5122874>.
- [13] N. Xia, D. Deng, X. Mu, A. Liu, J. Xie, D. Zhou, P. Yang, Y. Xing, L. Liu, Colorimetric immunoassays based on pyrroloquinoline quinone-catalyzed generation of Fe(II)-ferrozine with tris(2-carboxyethyl)phosphine as the reducing reagent, *Sensors Actuators B Chem.* 306 (2020) 127571, <https://doi.org/10.1016/j.snb.2019.127571>.
- [14] Y. Zhu, Y. Fang, S. Kaskel, Folate-conjugated Fe₃O₄@SiO₂ hollow mesoporous spheres for targeted anticancer drug delivery, *J. Phys. Chem. C* 114 (2010) 16382–16388, <https://doi.org/10.1021/jp106685q>.
- [15] H. Yang, Y. Li, T. Li, M. Xu, Y. Chen, C. Wu, X. Dang, Y. Liu, Multifunctional core/shell nanoparticles cross-linked polyetherimide-folic acid as efficient Notch-1 siRNA carrier for targeted killing of breast cancer, *Sci. Rep.* 4 (2015) 7072, <https://doi.org/10.1038/srep07072>.
- [16] Z. Xu, C. Shen, Y. Hou, H. Gao, S. Sun, Oleylamine as both reducing agent and stabilizer in a facile synthesis of magnetite nanoparticles, *Chem. Mater.* 21 (2009) 1778–1780, <https://doi.org/10.1021/cm802978z>.
- [17] J. Kim, J.E. Lee, J. Lee, J.H. Yu, B.C. Kim, K. An, Y. Hwang, C.-H. Shin, J.-G. Park, T. Hyeon, Magnetic fluorescent delivery vehicle using uniform mesoporous silica spheres embedded with monodisperse magnetic and semiconductor nanocrystals, *J. Am. Chem. Soc.* 128 (2006) 688–689, <https://doi.org/10.1021/ja0565875>.
- [18] X. Ma, Y. Zhao, K.W. Ng, Y. Zhao, Integrated hollow mesoporous silica nanoparticles for target drug/siRNA co-delivery, *Chem. - A Eur. J.* 19 (2013) 15593–15603, <https://doi.org/10.1002/chem.201302736>.
- [19] S. Shanehsazzadeh, M.A. Oghabian, B.J. Allen, M. Amanlou, A. Masoudi, F.J. Daha, Evaluating the effect of ultrasmall superparamagnetic iron oxide nanoparticles for a long-term magnetic cell labeling, *J. Med. Phys.* 38 (2013) 34–40, <https://doi.org/10.4103/0971-6203.106603>.
- [20] S. Sheng-Nan, W. Chao, Z. Zan-Zan, H. Yang-Long, S.S. Venkatramana, X. Zhi-Chuan, Magnetic iron oxide nanoparticles: synthesis and surface coating techniques for biomedical applications, *Chin. Phys. B* 23 (2014), <https://doi.org/10.1088/1674-1056/23/3/037503> 037503–1–037503–19.
- [21] Ö. Metin, Ş. Aydoğan, K. Meral, A new route for the synthesis of graphene oxide-Fe₃O₄ (GO-Fe₃O₄) nanocomposites and their Schottky diode applications, *J. Alloys Compd.* 585 (2014) 681–688, <https://doi.org/10.1016/j.jallcom.2013.09.159>.
- [22] H.-M. Yang, H.J. Lee, K.-S. Jang, C.W. Park, H.W. Yang, W. Do Heo, J.-D. Kim, Poly (amino acid)-coated iron oxide nanoparticles as ultra-small magnetic resonance probes, *J. Mater. Chem.* 19 (2009) 4566, <https://doi.org/10.1039/b820139k>.
- [23] R. Sharma, V. Kumar, S. Bansal, S. Singhal, Assortment of magnetic nanospinel for activation of distinct inorganic oxidants in photo-Fenton's process, *J. Mol. Catal. A Chem.* 402 (2015) 53–63, <https://doi.org/10.1016/j.molcata.2015.03.009>.
- [24] J. Zhang, X. Li, J.M. Rosenholm, H. Gu, Synthesis and characterization of pore size-tunable magnetic mesoporous silica nanoparticles, *J. Colloid Interface Sci.* 361 (2011) 16–24, <https://doi.org/10.1016/j.jcis.2011.05.038>.
- [25] T. Suteewong, H. Sai, J. Lee, M. Bradbury, T. Hyeon, S.M. Gruner, U. Wiesner, Ordered mesoporous silica nanoparticles with and without embedded iron oxide nanoparticles: structure evolution during synthesis, *J. Mater. Chem.* 20 (2010) 7807–7814, <https://doi.org/10.1039/c0jm01002b>.
- [26] R. Kumar, H.T. Chen, J.L.V. Escoto, V.S.Y. Lin, M. Pruski, Template removal and thermal stability of organically functionalized mesoporous silica nanoparticles, *Chem. Mater.* 18 (2006) 4319–4327, <https://doi.org/10.1021/cm060598v>.
- [27] A. Liberman, N. Mendez, W.C. Troglor, A.C. Kummel, Synthesis and surface functionalization of silica nanoparticles for nanomedicine, *Surf. Sci. Rep.* 69 (2014) 132–158, <https://doi.org/10.1016/j.surfrep.2014.07.001>.
- [28] X. Liu, Q. Chen, G. Yang, L. Zhang, Z. Liu, Z. Cheng, X. Zhu, Magnetic nanomaterials with near-infrared pH-activatable fluorescence via iron-catalyzed AGET ATRP for tumor acidic microenvironment imaging, *J. Mater. Chem. B* 3 (2015) 2786–2800, <https://doi.org/10.1039/c5tb00070j>.
- [29] B.K. Möller, J. Kobler, T. Bein, Colloidal suspensions of nanometer-sized Mesoporous silica, *Adv. Funct. Mater.* 17 (2007) 605–612, <https://doi.org/10.1002/adfm.200600578>.
- [30] W. Jiang, J. Wu, R. Tian, W. Jiang, Synthesis and characterization of magnetic mesoporous core-shell nanocomposites for targeted drug delivery applications, *J. Porous Mater.* 24 (2016) 257–265, <https://doi.org/10.1007/s10934-016-0259-z>.
- [31] Q. He, J. Shi, Mesoporous silica nanoparticle based nano drug delivery systems: synthesis, controlled drug release and delivery, *Mater. Chem.* 21 (2011) 5845–5855, <https://doi.org/10.1039/C0JM03851B>.
- [32] P.T. Yin, S. Shah, N.J. Pasquale, O.B. Garbuzenko, T. Minko, K.B. Lee, Stem cell-based gene therapy activated using magnetic hyperthermia to enhance the treatment of cancer, *Biomaterials* 81 (2016) 46–57, <https://doi.org/10.1016/j.biomaterials.2015.11.023>.
- [33] H. Fasehee, R. Dinarvand, A. Ghavamzadeh, M. Esfandyari-Manesh, H. Moradian, S. Faghihi, S.H. Ghaffari, Delivery of disulfiram into breast cancer cells using folate-receptor-targeted PLGA-PEG nanoparticles: in vitro and in vivo investigations, *J. Nanobiotechnology* 14 (2016) 32, <https://doi.org/10.1186/s12951-016-0183-z>.
- [34] H. Cai, X. An, J. Cui, J. Li, S. Wen, K. Li, M. Shen, L. Zheng, G. Zhang, X. Shi, Facile hydrothermal synthesis and surface functionalization of polyethyleneimine-coated iron oxide nanoparticles for biomedical applications, *ACS Appl. Mater. Interfaces* 5 (2013) 1722–1731, <https://doi.org/10.1021/am302883m>.
- [35] R.V. Benjaminsen, M.A. Matthejerg, J.R. Henriksen, S.M. Moghimi, T.L. Andresen, The possible “proton sponge” effect of polyethyleneimine (PEI) does not include change in lysosomal pH, *Mol. Ther.* 21 (2013) 149–157, <https://doi.org/10.1038/mt.2012.185>.
- [36] N. Parker, M.J. Turk, E. Westrick, J.D. Lewis, P.S. Low, C.P. Leamon, Folate receptor expression in carcinomas and normal tissues determined by a quantitative radioligand binding assay, *Anal. Biochem.* 338 (2005) 284–293, <https://doi.org/10.1016/j.ab.2004.12.026>.
- [37] R. Han, H. Yi, J. Shi, Z. Liu, H. Wang, Y. Hou, Y. Wang, pH-responsive drug release and NIR-triggered singlet oxygen generation based on a multifunctional core-shell-shell structure, *Phys. Chem. Chem. Phys.* 18 (2016) 25497–25503, <https://doi.org/10.1039/c6cp05308d>.
- [38] M.S. Islam, W.S. Choi, H.J. Lee, Controlled etching of internal and external

- structures of SiO₂ nanoparticles using hydrogen bond of polyelectrolytes, *ACS Appl. Mater. Interfaces* 6 (2014) 9563–9571, <https://doi.org/10.1021/am501941c>.
- [39] C. Argyo, V. Weiss, C. Bräuchle, T. Bein, Multifunctional mesoporous silica nanoparticles as a universal platform for drug delivery, *Chem. Mater.* 26 (2014) 435–451, <https://doi.org/10.1021/cm402592t>.
- [40] P. Liu, I.S. Kumar, S. Brown, V. Kannappan, P.E. Tawari, J.Z. Tang, W. Jiang, A.L. Armesilla, J.L. Darling, W. Wang, Disulfiram targets cancer stem-like cells and reverses resistance and cross-resistance in acquired paclitaxel-resistant triple-negative breast cancer cells, *Br. J. Cancer* 109 (2013) 1876–1885, <https://doi.org/10.1038/bjc.2013.534>.
- [41] L. Zhang, B. Tian, Y. Li, T. Lei, J. Meng, L. Yang, Y. Zhang, F. Chen, H. Zhang, H. Xu, Y. Zhang, X. Tang, A copper-mediated disulfiram-loaded pH-triggered PEG-shedding TAT peptide-modified lipid nanocapsules for use in tumor therapy, *ACS Appl. Mater. Interfaces* 7 (2015) 25147–25161, <https://doi.org/10.1021/acsami.5b06488>.
- [42] M. Najlah, Z. Ahmed, M. Iqbal, Z. Wang, P. Tawari, W. Wang, C. McConville, Development and characterisation of disulfiram-loaded PLGA nanoparticles for the treatment of non-small cell lung cancer, *Eur. J. Pharm. Biopharm.* 112 (2016) 224–233, <https://doi.org/10.1016/j.ejpb.2016.11.032>.
- [43] W. Song, Z. Tang, N. Shen, H. Yu, Yanjie Jia, D. Zhang, J. Jiang, C. He, H. Tian, X. Chen, Combining disulfiram and poly(L-glutamic acid)-cisplatin conjugates for combating cisplatin resistance, *J. Control. Release* 231 (2016) 94–102, <https://doi.org/10.1016/j.jconrel.2016.02.039>.
- [44] W. Song, Z. Tang, T. Lei, X. Wen, G. Wang, D. Zhang, M. Deng, X. Tang, X. Chen, Stable loading and delivery of disulfiram with mPEG-PLGA/PCL mixed nanoparticles for tumor therapy, *Nanomedicine: Nanotechnology, Biol. Med* 12 (2016) 377–386, <https://doi.org/10.1016/j.nano.2015.10.022>.
- [45] Z. Wei, Y. Wu, Y. Zhao, L. Mi, J. Wang, J. Wang, J. Zhao, L. Wang, A. Liu, Y. Li, W. Wei, Y. Zhang, S. Liu, Multifunctional nanoprobe for cancer cell targeting and simultaneous fluorescence/magnetic resonance imaging, *Anal. Chim. Acta* 938 (2016) 156–164, <https://doi.org/10.1016/j.aca.2016.07.037>.
- [46] T. Li, X. Shen, Y. Chen, C. Zhang, J. Yan, H. Yang, C. Wu, H. Zeng, Y. Liu, Polyetherimide-grafted Fe₃O₄@SiO₂ nanoparticles as theranostic agents for simultaneous VEGF siRNA delivery and magnetic resonance cell imaging, *Int. J. Nanomedicine* 10 (2015) 4279–4291, <https://doi.org/10.2147/IJN.S85095>.
- [47] J. Soleymani, M. Hasanzadeh, M.H. Somi, N. Shadjou, A. Jouyban, Probing the specific binding of folic acid to folate receptor using amino-functionalized mesoporous silica nanoparticles for differentiation of MCF 7 tumoral cells from MCF 10A, *Biosens. Bioelectron.* 115 (2018) 61–69, <https://doi.org/10.1016/j.bios.2018.05.025>.
- [48] N. Nagai, M. Inomata, Y. Ito, Contribution of aldehyde dehydrogenase 3A1 to disulfiram penetration through monolayers consisting of cultured human corneal epithelial cells, *Biol. Pharm. Bull.* 31 (2008) 1444–1448, <https://doi.org/10.1248/bpb.31.1444>.
- [49] M. Viola-Rhenals, M.S. Rieber, M. Rieber, Suppression of survival in human SKBR3 breast carcinoma in response to metal-chelator complexes is preferential for copper-dithiocarbamate, *Biochem. Pharmacol.* 71 (2006) 722–734, <https://doi.org/10.1016/j.bcp.2005.11.028>.
- [50] H.Y. Cho, A. Mavi, S.T.D. Chueng, T. Pongkulapa, N. Pasquale, H. Rabie, J. Han, J.H. Kim, T.H. Kim, J.W. Choi, K.B. Lee, Tumor homing reactive oxygen species nanoparticle for enhanced cancer therapy, *ACS Appl. Mater. Interfaces* 11 (2019) 23909–23918, <https://doi.org/10.1021/acsami.9b07483>.
- [51] P.E. Tawari, Z. Wang, M. Najlah, C.W. Tsang, V. Kannappan, P. Liu, C. McConville, B. He, A.L. Armesilla, W. Wang, The cytotoxic mechanisms of disulfiram and copper (II) in cancer cells Patricia, *Toxicol. Res.* 4 (2015) 1439–1442, <https://doi.org/10.1039/C5TX00210A>.
- [52] X. Lun, J.C. Wells, N. Grinshtein, J.C. King, X. Hao, N.H. Dang, X. Wang, A. Aman, D. Uehling, A. Datti, J.L. Wrana, J.C. Easaw, A. Luchman, S. Weiss, J.G. Cairncross, D.R. Kaplan, S.M. Robbins, D.L. Senger, Disulfiram when combined with copper enhances the therapeutic effects of temozolomide for the treatment of glioblastoma, *Clin. Cancer Res.* 22 (2016) 3860–3875, <https://doi.org/10.1158/1078-0432.CCR-15-1798>.
- [53] T. Kaku, M.H. Jiang, J. Hada, K. Morimoto, Y. Hayashi, Sodium nitroprusside-induced seizures and adenosine release in rat hippocampus, *Eur. J. Pharmacol.* 413 (2001) 199–205, [https://doi.org/10.1016/S0014-2999\(01\)00763-4](https://doi.org/10.1016/S0014-2999(01)00763-4).
- [54] M.V. Rhenals, M. Strasberg-Rieber, M. Rieber, Nitric oxide donors or nitrite counteract copper-[dithiocarbamate] 2-mediated tumor cell death and inducible nitric oxide synthase down-regulation: possible role of a nitrosyl-copper [dithiocarbamate] 2 complex, *J. Med. Chem.* 53 (2010) 1627–1635, <https://doi.org/10.1021/jm901314r>.
- [55] P. Liu, Z. Wang, S. Brown, V. Kannappan, P.E. Tawari, W. Jiang, J.M. Irache, J.Z. Tang, A.L. Armesilla, J.L. Darling, X. Tang, W. Wang, Liposome encapsulated disulfiram inhibits NFκB pathway and targets breast cancer stem cells in vitro and in vivo, *Oncotarget* 5 (2014) 7471–7485, <https://doi.org/10.18632/oncotarget.2166>.
- [56] L. Duan, H. Shen, G. Zhao, R. Yang, X. Cai, L. Zhang, C. Jin, Y. Huang, Inhibitory effect of disulfiram/copper complex on non-small cell lung cancer cells, *Biochem. Biophys. Res. Commun.* 446 (2014) 1010–1016, <https://doi.org/10.1016/j.bbrc.2014.03.047>.
- [57] J.L. Allensworth, M.K. Evans, F. Bertucci, A.J. Aldrich, R.A. Festa, P. Finetti, N.T. Ueno, R. Safi, D.P. McDonnell, D.J. Thiele, S. Van Laere, G.R. Devi, Disulfiram (DSF) acts as a copper ionophore to induce copper-dependent oxidative stress and mediate anti-tumor efficacy in inflammatory breast cancer, *Mol. Oncol.* 9 (2015) 1155–1168, <https://doi.org/10.1016/j.molonc.2015.02.007>.
- [58] Y. Yang, Q. Deng, X. Feng, J. Sun, Use of the disulfiram/copper complex for breast cancer chemoprevention in MMTV-erbB2 transgenic mice, *Mol. Med. Rep.* 12 (2015) 746–752, <https://doi.org/10.3892/mmr.2015.3426>.
- [59] S.P. Verma, B.R. Goldin, Copper modulates activities of genistein, nitric oxide, and curcumin in breast tumor cells, *Biochem. Biophys. Res. Commun.* 310 (2003) 104–108, <https://doi.org/10.1016/j.bbrc.2003.08.124>.